Radiology

REVIEWS AND COMMENTARY • REVIEW

Deep Learning Image Reconstruction for CT: Technical Principles and Clinical Prospects

*Lennart R. Koetzier, BSc** • *Domenico Mastrodicasa, MD** • *Timothy P. Szczykutowicz, PhD* • *Niels R. van der Werf, PhD* • *Adam S. Wang, PhD* • *Veit Sandfort, MD* • *Aart J. van der Molen, MD* • *Dominik Fleischmann, MD* • *Martin J. Willemink, MD, PhD*

From the Department of Radiology (L.R.K., D.M., A.S.W., V.S., D.F., M.J.W.) and Stanford Cardiovascular Institute (D.M., D.F., M.J.W.), Stanford University School of Medicine, 300 Pasteur Dr, Stanford, CA 94305-5105; Department of Radiology, University of Wisconsin–Madison, School of Medicine and Public Health, Madison, Wis (T.P.S.); Department of Radiology, Erasmus Medical Center, Rotterdam, the Netherlands (N.R.v.d.W.); Clinical Science Western Europe, Philips Healthcare, Best, the Netherlands (N.R.v.d.W.); and Department of Radiology, Leiden University Medical Center, Leiden, the Netherlands (A.J.v.d.M.). Received May 27, 2022; revision requested July 25; revision received September 26; accepted October 13. **Address correspondence to** M.J.W. (email: *m.j.willemink@gmail.com*).

* L.R.K. and D.M. contributed equally to this work.

Conflicts of interest are listed at the end of this article.

Radiology 2023; 306(3):e221257 • https://doi.org/10.1148/radiol.221257 • Content codes: CT AI

Filtered back projection (FBP) has been the standard CT image reconstruction method for 4 decades. A simple, fast, and reliable technique, FBP has delivered high-quality images in several clinical applications. However, with faster and more advanced CT scanners, FBP has become increasingly obsolete. Higher image noise and more artifacts are especially noticeable in lower-dose CT imaging using FBP. This performance gap was partly addressed by model-based iterative reconstruction (MBIR). Yet, its "plastic" image appearance and long reconstruction times have limited widespread application. Hybrid iterative reconstruction partially addressed these limitations by blending FBP with MBIR and is currently the state-of-the-art reconstruction technique. In the past 5 years, deep learning reconstruction (DLR) techniques have become increasingly popular. DLR uses artificial intelligence to reconstruct high-quality images from lower-dose CT faster than MBIR. However, the performance of DLR algorithms relies on the quality of data used for model training. Higher-quality training data will become available with photon-counting CT scanners. At the same time, spectral data would greatly benefit from the computational abilities of DLR. This review presents an overview of the principles, technical approaches, and clinical applications of DLR, including metal artifact reduction algorithms. In addition, emerging applications and prospects are discussed.

In CT, image reconstruction transforms projection data acquired from multiple angles into images by means of a mathematical process. Image reconstruction plays an integral role in improving diagnostic image quality by keeping noise and artifacts to a minimum while preserving spatial resolution (1). This has been done iteratively and analytically. In 1970, Gordon et al (2) introduced the first iterative reconstruction (IR) technique. However, due to the lack of computational power, a simpler analytical technique, named filtered back projection (FBP), dominated the reconstruction process for 40 years (3). Over time, the advancement of CT scanners—coupled with a growing commitment to keep radiation exposure as low as reasonably achievable (commonly referred to as ALARA)—led FBP into obsolescence. This was revealed by disproportionally higher image noise and artifacts when lowering the radiation dose with use of FBP (3,4). This shortcoming was addressed once computational abilities advanced in the 2000s, effectively allowing for the development of two types of IR algorithms: model-based IR (MBIR) and hybrid IR (HIR) (5). MBIR and HIR removed noise and artifacts, resulting in high-quality images, even in lower-dose protocols. However, other drawbacks related to noise texture and reconstruction time arose (6).

In the past 5 years, deep learning reconstruction (DLR) has been introduced to further improve image quality and possibly reduce radiation dose. DLR algorithms have the potential to outperform current reconstruction techniques. DLR achieves this by lowering image noise and artifacts while preserving spatial resolution and shortening reconstruction times, but its performance is only as good as the quality of the data used for its development.

In this review, we present an overview of the principles, technical approaches, and clinical applications of DLR for noise and artifact reduction. In addition, we discuss emerging applications, challenges, and prospects.

Evolution of Image Reconstruction

Filtered Back Projection

FBP has been the most commonly used reconstruction technique due to its computational efficiency and numeric stability (Fig 1) (3). FBP relies on several assumptions to simplify the reconstruction process, such as a point detector and pencil x-ray beam geometry. Although FBP is relatively simple, it performs adequately in most clinical situations. However, when the radiation dose is reduced or larger patients are scanned, the limitations of FBP become more evident in the form of higher noise and more artifacts (3). This behavior is explained by the simplified approximations of the CT raw data (also known as a sinogram: all different projections for each imaging section, which are then stacked together) acquired by FBP. Consequently, measurement errors due to the nonideal properties of the CT system (eg, detector cross-talk, beam hardening) cannot be taken into account (7).

Abbreviations

CNN = convolutional neural network, DLR = deep learning reconstruction, FBP = filtered back projection, FDA = U.S. Food and Drug Administration, HIR = hybrid IR, IR = iterative reconstruction, MAR = metal artifact reduction, MBIR = model-based IR

Summary

The clinical introduction of deep learning reconstruction (DLR) algorithms over the past 5 years has demonstrated the potential of DLR to rapidly reconstruct images with low noise, desired noise texture, and preserved spatial resolution while providing the opportunity to reduce radiation dose up to 71%.

Essentials

- Deep learning reconstruction (DLR) algorithms can be applied in the raw data domain, image domain, or both.
- Compared with filtered back projection and hybrid iterative reconstruction (HIR), DLR provides improved image quality.
- DLR potentially allows for radiation dose reductions between 30% and 71% compared with HIR while maintaining diagnostic image quality due to improved noise reduction.
- Deep learning–based metal artifact reduction (MAR) has the potential to remove metal artifacts more accurately than current state-of-the-art MAR methods.

Model-based Iterative Reconstruction

To overcome the limitations of FBP, MBIR was introduced for clinical use in 2009 (3). MBIR is the most computationally demanding type of IR because it uses multiple iterations of forward and back projections between the sinogram domain and image domain to optimize image quality (Fig 1). Models of the acquisition process, noise statistics, and system geometry reconstruct the projections as accurately as possible (8). The more complete model of MBIR allows for more reduction of noise and artifacts than FBP does (5). However, the high computational requirements and long reconstruction times of MBIR have limited its widespread clinical application (3,9).

Hybrid Iterative Reconstruction

To overcome the computational burden of MBIR, HIR was developed (3). HIR consists of iterations in the sinogram domain, one back projection, and more iterations in the image domain (Fig 1). One back projection is less computationally demanding but also less capable of noise and artifact reduction than MBIR (5).

Finally, both approaches have a common limitation with respect to noise texture. Image noise can be measured as the standard deviation of Hounsfield units within a homogeneous

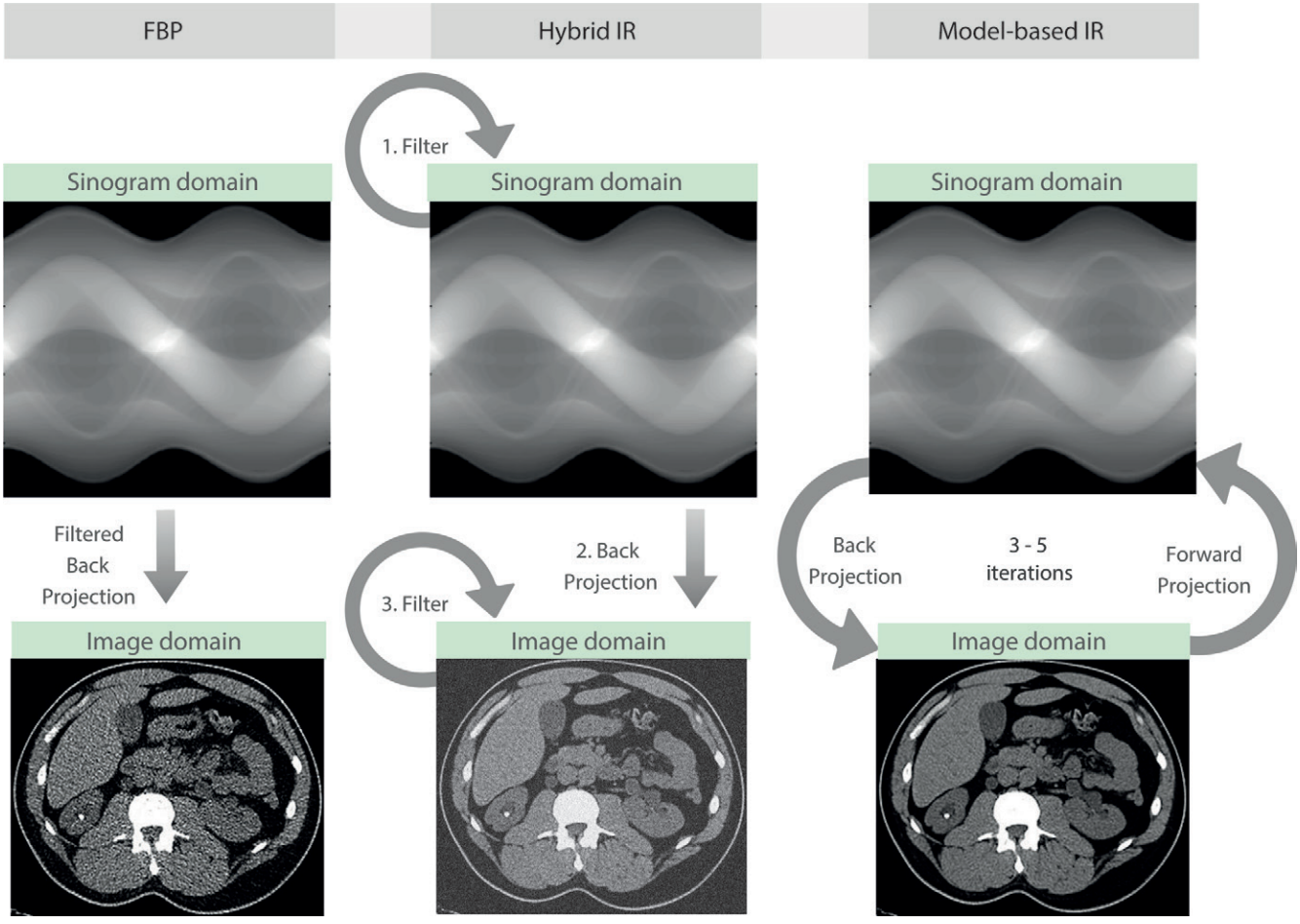

Figure 1: Overview of filtered back projection (FBP), hybrid iterative reconstruction (IR), and model-based IR. With FBP, projection data (sinograms) are filtered by a high-pass filter and subsequently backward-projected into the image domain (left column). In hybrid IR, the sinograms are iteratively filtered to reduce artifacts and backward-projected into the image domain; then, images are iteratively filtered to reduce image noise (middle column). With model-based IR, sinograms are backward-projected into the image domain. Subsequently, with use of models of the acquisition process, images are forward-projected into the sinogram domain to generate artificial sinograms. The artificial sinograms are compared with the true sinograms to thereupon optimize images and remove image noise. This process usually takes three to five iterations (right column).

region of interest. Both MBIR and HIR result in reduced image noise. However, using standard deviation to define image noise does not capture differences in noise texture. The low-frequency noise of MBIR and HIR images is often described as "plastic" or "blotchy" and hampers the detectability of low-contrast tissue interfaces (Fig 2) (10).

Principles of Deep Learning

The substantial growth of artificial intelligence in medical imaging shows the high interest in this subject. Because of this, background knowledge about the principles of artificial intelligence and deep learning is assumed. Examples of principles related to DLR are feature engineering, convolutional neural networks (CNNs), nodes and layers, forward and backward propagation, weight adjustment, training, validation, and testing (Figs 3, 4). We encourage readers to review these principles before continuing (11–14). The next paragraphs elaborate on the use of deep learning in image reconstruction, specifically in regard to noise, radiation, and artifact reduction.

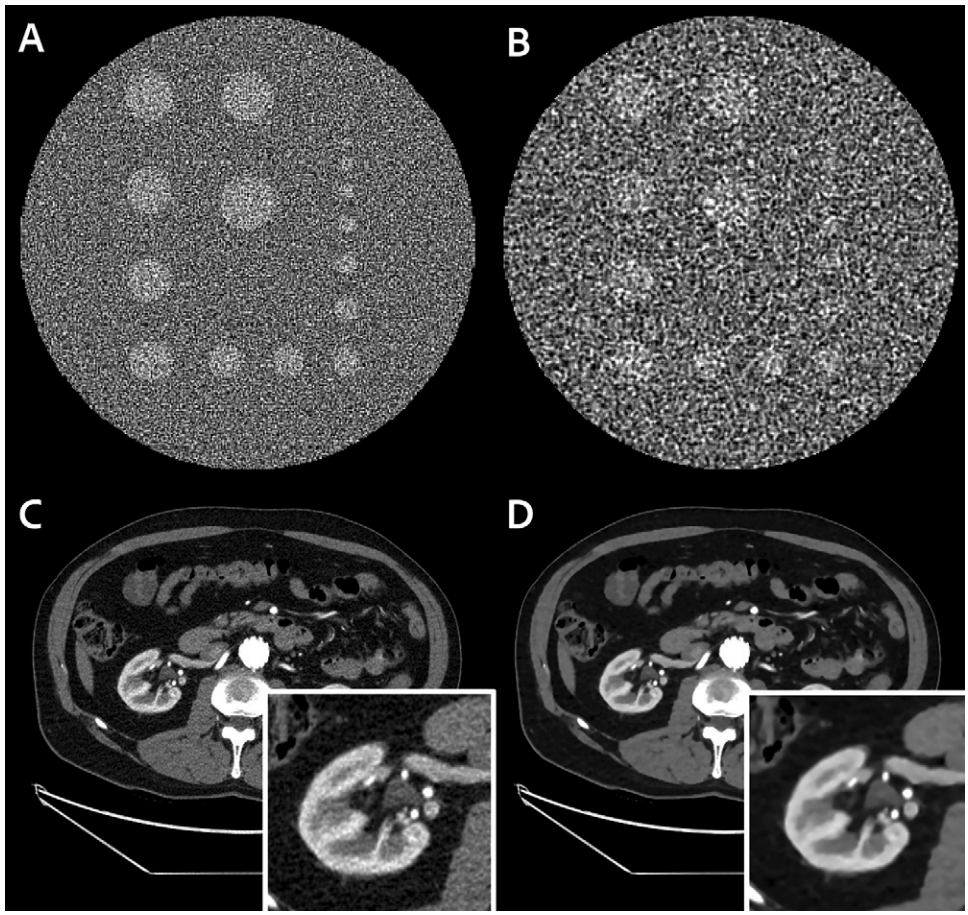

Figure 2: Examples of how noise texture changes can alter image appearance in objectionable ways. In this example, a phantom scan was acquired with equal noise magnitude (noise standard deviation), but with **(A)** a lower-frequency and **(B)** higher-frequency reconstruction kernel. In reconstruction **B**, where the noise texture is similar in length scale to the small objects inside the phantom, detection of those objects is difficult. **(C, D)** A clinical example using a commercial iterative reconstruction solution demonstrates the same principle. In this case, the noise level diminishes moving from reconstruction **C** to **D**, but with a major change in noise texture. Reconstruction **D** is said to have a "plastic," "blotchy," or "coarse" graininess compared with reconstruction **C**, which many radiologists find objectionable, as it mimics pathologic abnormalities or hinders detection of small, low-contrast objects.

Deep Learning–based CT Image Reconstruction

Indirect and Direct DLR Frameworks

In the past 5 years, multiple deep learning–based reconstruction methods have been described (15–17). These methods can be grouped into two categories: indirect and direct DLR frameworks. These categories are distinguished based on the use of FBP or IR (Fig 5).

Indirect DLR

In indirect DLR frameworks, either FBP or IR is used. The three types of indirect frameworks are differentiated based on when the deep learning network is deployed. These are sinogram-based, image-based, and hybrid frameworks. Sinogram-based frameworks focus on sinogram optimization, and the network is deployed before the sinogram undergoes FBP or IR. In image-based frameworks, the network optimizes the image after initial reconstruction with FBP or IR. Hybrid frameworks combine sinogram and image optimization.

In indirect reconstruction, deep learning networks are commonly CNN-based. Two examples are wavelet transform–based U-Net (18) and residual encoder-decoder CNN (19). Transformer-based neural networks and generative adversarial networks (20) are examples of a non-CNN–based approach to image optimization (21).

Direct DLR

Direct DLR algorithms reconstruct the sinogram directly into an image, without the use of FBP or IR (Fig 5). This potentially reduces artifacts introduced by FBP or IR. However, this is only possible if the ground truth images used for model training do not contain FBP- or IR-related artifacts. Examples of direct algorithms include AUTOMAP and iRadonMAP (22,23).

Building a DLR Model

A core component of DLR model development is the setting and tuning of hyperparameters, such as network structure, number of layers, and activation function. These features must be established early because they cannot be learned during the training process.

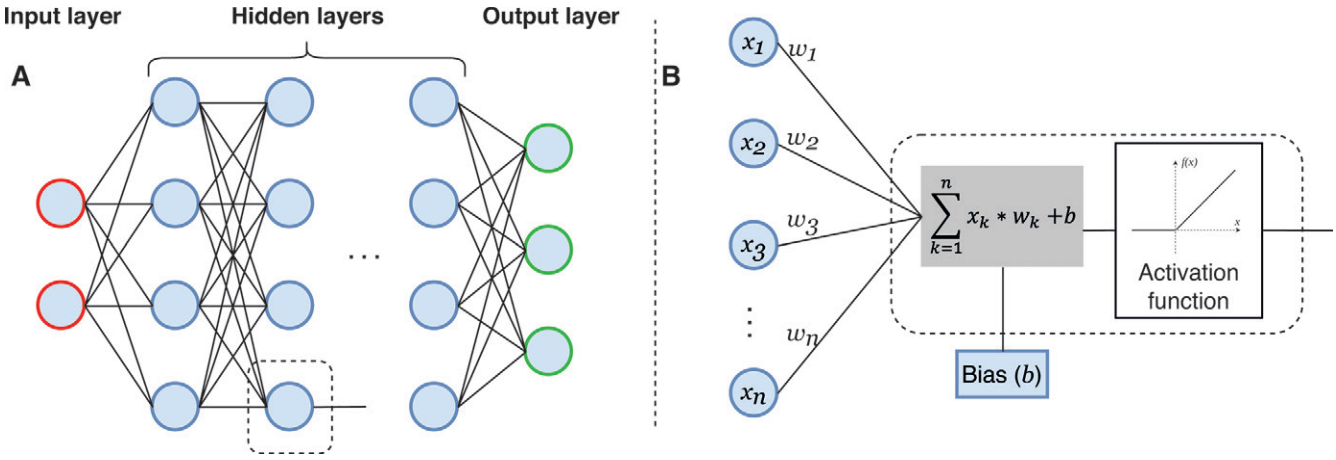

Figure 3: Schematic structure of a deep learning network. **(A)** Diagram shows the input layer, multiple hidden layers, and output layer. Previous and subsequent layers are connected through nodes. **(B)** Input of a node consists of the bias (*b*) and output (x_n) from multiple nodes from the previous layer multiplied by its weight (w_n). The sum of the input is passed through an activation function.

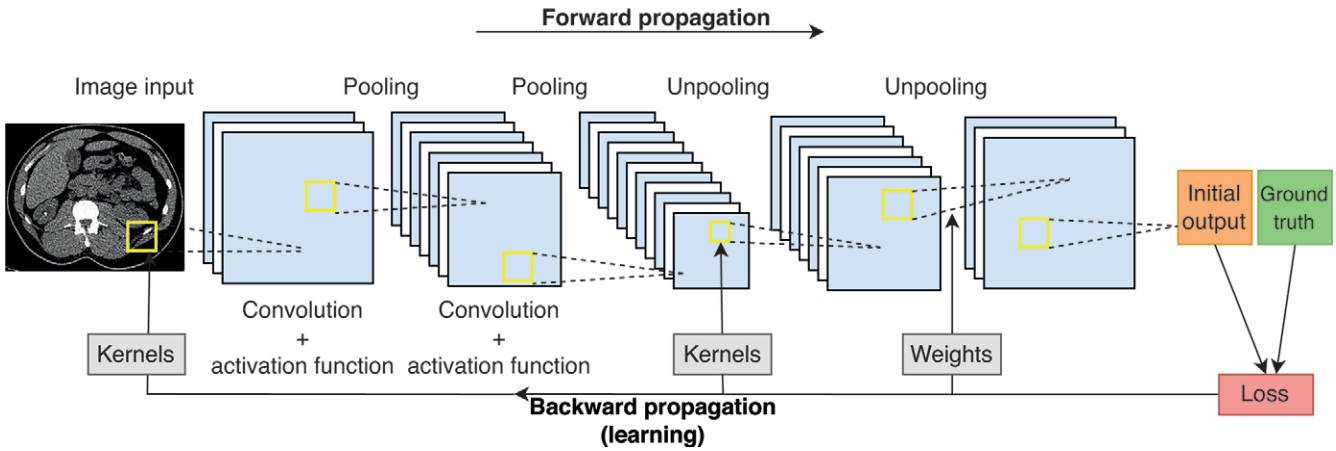

Figure 4: Schematic structure of convolutional neural network in training. During forward propagation, kernels in convolutional layers identify features in the input, and features are passed through an activation function. Pooling the layers reduces the amount of computation performed in the network. During training, the network compares initial output and ground truth in a loss function. Finally, kernels and weights are iteratively adjusted in the backward propagation.

Subsequently, the network undergoes training, validation, and testing phases (Fig 6). Ideally, DLR models are trained using lower-dose CT data as input and matched to routine- (roughly two to four times the lower-dose) or higher-dose (roughly four to eight times the lower-dose) CT data as the ground truth information. The use of matched data makes the training process "supervised" (24). Additionally, when DLR algorithms are trained on data with substantial artifacts as input and low-artifact data as ground truth, images can potentially be reconstructed with reduced artifacts. The detection and removal of artifacts in the sinogram domain are more efficient than image-based artifact reduction (3). Therefore, artifact reduction is expected to be better with direct followed by indirect reconstruction algorithms, including hybrid, sinogram-based, and image-based.

Currently Available Deep Learning Algorithms

To date, three CT vendors and two independent (vendor-agnostic) software companies have released DLR algorithms approved by the U.S. Food and Drug Administration (FDA) (25–29) (Table 1).

TrueFidelity.—In 2019, TrueFidelity (GE Healthcare) became the first DLR technique approved by the FDA (25). Input data for the training phase consisted of lower-dose sinograms acquired in both phantoms and patients. From the lower-dose sinograms, a direct DLR model used a CNN to generate estimations of the reconstructed image. These estimations were compared with higher-than-routine-dose images reconstructed with FBP, which served as the ground truth (25). Because TrueFidelity was trained on FBP images, the resulting images retain FBP-like noise texture, sharpness, and artifact properties (30).

AiCE.—The second DLR algorithm approved by the FDA was Advanced Intelligent Clear-IQ Engine (or AiCE, Canon Medical Systems) in 2019 (27). The algorithm is based on a CNN trained with patient data consisting of lower-dose HIR images as input and routine-dose full MBIR images as ground truth. Besides noise reduction, MBIR as ground truth allows for artifact reduction because of its ability to model system optics, system physics, scanner statistical properties, and human anatomy. An additional advantage of using MBIR is that more iterations can

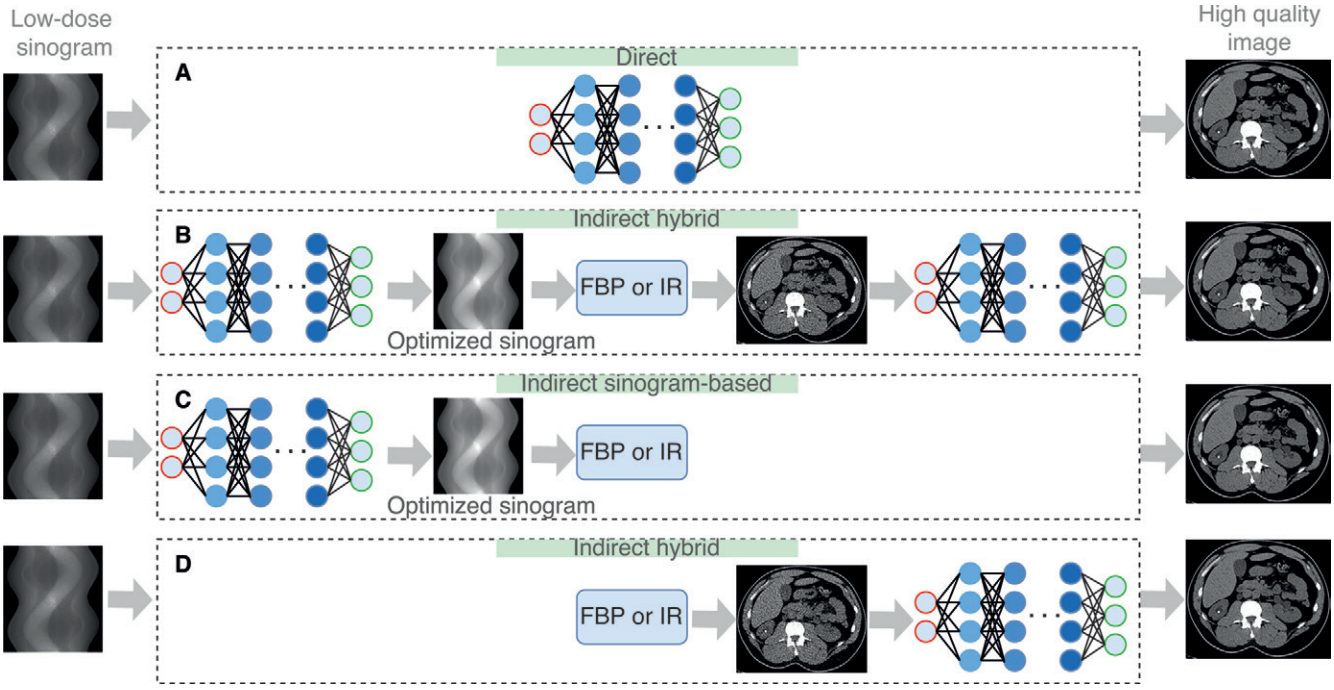

Figure 5: Diagram shows overview of different deep learning reconstruction (DLR) types. **(A)** Direct DLR algorithms reconstruct a high-quality image directly from the sinogram without filtered back projection (FBP) or iterative reconstruction (IR). **(B)** The indirect hybrid method uses both optimization in the sinogram and image domain and FBP or IR step to create a high-quality image. **(C)** The indirect sinogram-based method only optimizes the sinogram before reconstruction with FBP or IR. **(D)** The indirect image-based method first reconstructs an image with FBP or IR before optimization in the image domain.

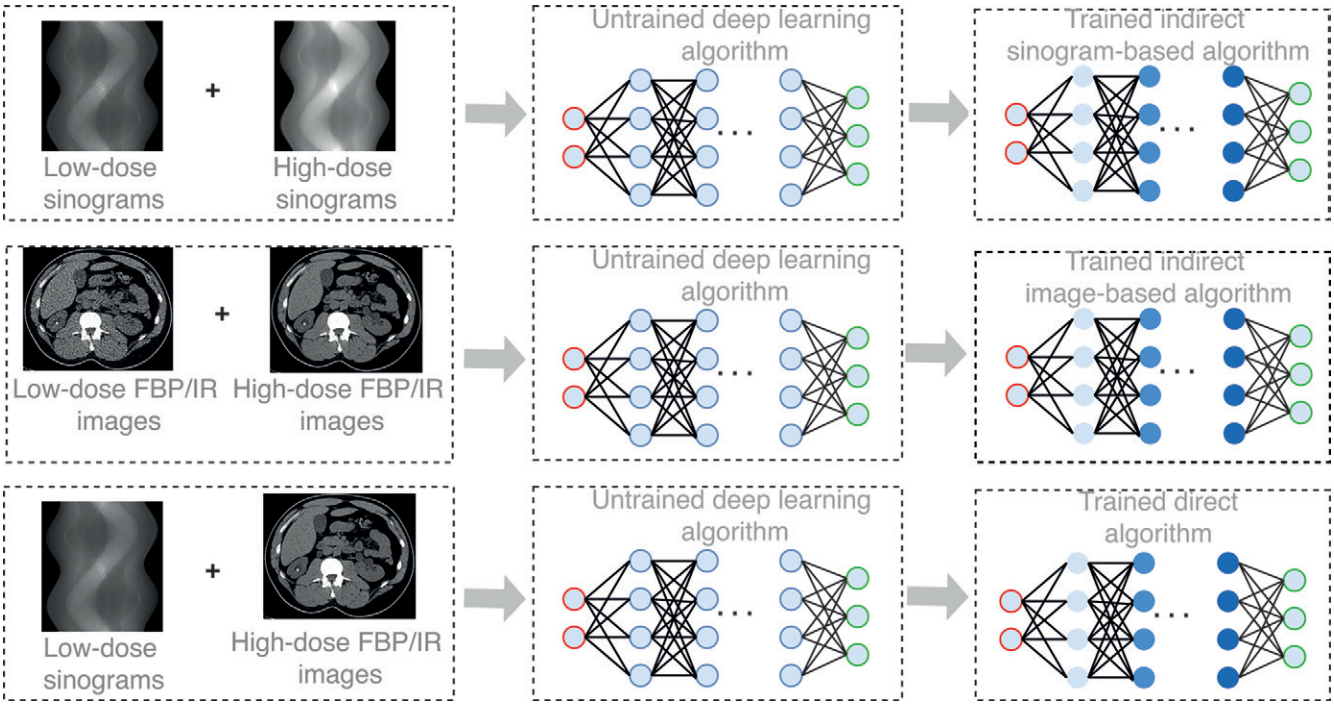

Figure 6: Schematic overview of deep learning reconstruction (DLR) training. Different pairs of input data and ground truth result in different DLR types. FBP = filtered back projection, IR = iterative reconstruction.

be used in the training phase than in a time-constrained clinical setting. More iterations potentially allow for higher-quality ground truth images and better DLR performance (27,31).

This indirect, image-based DLR algorithm starts by filtering the sinogram, taking into account information about the scanner model, such as gantry size and detector materials. Then, it reconstructs an initial image by using HIR. This image is subsequently fed into the CNN, which delivers an improved image as output (32,33). Because images are reconstructed with HIR and then fed into a fast deep learning

Table 1: Currently Commercially Available Deep Learning Algorithms

Algorithm Name	Algorithm Developer	Algorithm Class	Algorithm Type	Ground Truth Images
TrueFidelity	GE Healthcare	DLR	Direct	FBP
AiCE	Canon Medical Systems	DLR	Indirect, image-based	MBIR
Precise Image	Philips Healthcare	DLR	Direct	FBP
PixelShine	AlgoMedica	DLD	Image denoiser	FBP, HIR, MBIR
ClariCT.AI	ClariPi	DLD	Image denoiser	FBP

Note.—AiCE = Advanced Intelligent Clear-IQ Engine, DLR = deep learning reconstruction, DLD = deep learning–based denoiser, FBP = filtered back projection, HIR = hybrid iterative reconstruction, MBIR = model-based iterative reconstruction.

algorithm, reconstruction times per scan of this DLR are slightly longer than with HIR (44 seconds vs 27 seconds, respectively, for brain scans) (34). Nonetheless, reconstruction times of DLR are still three to five times shorter than those of MBIR (9,31,33).

Precise Image.—More recently, a third vendor released a direct DLR algorithm (Precise Image, Philips Healthcare), which was approved by the FDA in 2022 (26). In this algorithm, a CNN was trained on lower-dose-simulated sinograms (input) and matched routine-dose FBP images as ground truth. Simulated noise was added before reconstruction. The network was trained on patient data obtained from different patient groups and populations with a variety of scan parameters (26). To our knowledge, public information about this algorithm is unavailable except for a white paper (26).

Overall, DLR resulted in shorter reconstruction times than MBIR, thus potentially leading to optimized workflow (34). Because vendor-specific reconstruction algorithms are proprietary, technical details are usually not provided. This makes it difficult to interpret certain image characteristics or artifacts that may be caused by DLR. In addition, the aforementioned vendor-specific DLR algorithms currently operate only on a few high-end CT scanner models.

ClariCT.AI and PixelShine.—To overcome the limitations of a vendor-specific solution for image reconstruction, two software companies developed deep learning–based denoising (DLD) algorithms, both of which operate on reconstructed images (28,29). Both denoising algorithms, ClariCT.AI (ClariPi) and PixelShine (AlgoMedica), obtained FDA clearance in 2019. For the training process, ClariCT.AI used noise-simulated FBP images as input and the original routine-dose FBP images as ground truth (28). PixelShine used a mixture of lower-dose FBP, HIR, and MBIR images as input and routine-dose FBP images as ground truth (29). Both algorithms were trained on over a million CT images acquired on scanners across four CT vendors (Canon Medical Systems, GE Healthcare, Philips Healthcare, and Siemens Healthineers) using several combinations of reconstruction parameters (28,35). Nam and colleagues (35) compared the subjective image quality of ClariCT.AI and HIR on 100 lower-dose follow-up chest CT scans. Noise appearance, spatial resolution, and overall image quality of ClariCT.AI were superior to those of HIR. Hata et al (36) compared lower-dose chest CT images reconstructed with FBP-PixelShine, HIR-PixelShine, and MBIR-PixelShine combinations with standalone FBP, HIR, or MBIR, respectively. With PixelShine, noise, streak artifacts, and overall image quality improved for all comparisons.

Notwithstanding the improvement in image quality, deep learning–based denoising algorithms have been tested only on streak artifacts. Other artifacts, such as beam hardening, are better corrected in the sinogram domain (3); hence, it is fair to expect that denoising algorithm performance in artifact reduction is limited.

Image Quality of DLR

Because the quality of an image is determined by several components, it is often difficult to measure image quality in a single metric. Therefore, objective metrics such as noise magnitude, signal-to-noise ratio, contrast-to-noise ratio, and structural similarity are used to quantify and compare the image quality of reconstruction techniques. Additionally, in observer studies, radiologists subjectively rate the components of image quality, such as noise, sharpness, and artifact presence.

Image Noise

Image noise in DLR images is often compared with thick-section and routine-dose HIR images as a reference: *(a)* in routine-dose protocols, DLR delivers higher image quality; *(b)* in lower-dose CT scans, DLR improves image quality by reducing image noise to a level comparable with that of the reference; *(c)* in thin-section images, routine-dose DLR reduces image noise to a level comparable with that of the reference.

Image Noise in Routine-Dose Protocols

Image noise metrics were investigated either only objectively (noise magnitude [standard deviation], signal-to-noise ratio, and contrast-to-noise ratio) (Table 2) or both objectively and subjectively. Most studies describing objective image quality performances of DLR algorithms reported significant noise reduction compared with FBP, HIR, or MBIR at similar or lower dose levels (37–40). In image quality studies including both objective and subjective evaluations, if image noise was objectively assessed as low, readers would also score image noise as low. This resulted in better overall image quality scores (34,41–45). For example, Oostveen et al (34) compared the objective and subjective image quality of HIR, MBIR, and DLR images in 50 patients who underwent brain CT. Noise magnitude (standard deviation) was lower in DLR

Table 2: Noteworthy Studies on Deep Learning Reconstruction for CT Imaging

Author	Year	DLR Name	Application	Study Type	No. of Patients	Objective Metrics	Main Finding
Oostveen et al (34)	2021	AiCE	Brain	Patient	50	SD, SNR	Compared with HIR, DLR of cerebral noncontrast CT results in lower noise and improved tissue differentiation
Kim et al (53)	2021	TrueFidelity	Brain	Patient	62	SD, CNR, AI	Compared with HIR, DLR allowed noise and artifact reduction with improved subjective image quality
Masuda et al (92)	2022	TrueFidelity	Dual-energy CT	Phantom	NA	SD, NPS, SP	The spatial resolution of VMS-DLR images varied significantly depending on the contrast
Sato et al (93)	2022	TrueFidelity	Abdomen (dual-energy CT)	Patient	26	SD, CNR	Compared with HIR, DLR improved conspicuity of abdominal solid lesions on VMS images
Li et al (94)	2022	TrueFidelity	Heart	Patient	100	SD, CNR, SNR	Compared with HIR, DLR allowed radiation dose and contrast medium reduction in aortic CT angiography
Bernard et al (74)	2021	AiCE	Heart	Patient	296	SD, SNR, CNR	Compared with HIR, DLR reduced radiation dose by 40% while increasing SNR and CNR by 50% in cardiac CT angiography
Benz et al (46)	2022	TrueFidelity	Heart	Patient	50	SD, SNR, CNR	Compared with HIR, DLR reduced radiation dose in coronary CT angiography by 43% without impact on noise, stenosis severity, plaque composition, or quantitative plaque volume
Yi et al (95)	2021	AiCE	Heart	Patient	42	SD, CNR, SNR	Compared with HIR, DLR improved image quality in coronary CT angiography and diagnostic performance for calcification-related obstructive coronary artery disease
Benz et al (75)	2020	TrueFidelity	Heart	Patient	43	SD	Compared with HIR, DLR reduced noise in coronary CT angiography while yielding superior image quality at equal diagnostic accuracy
Higaki et al (72)	2020	AiCE	Image characteristics	Phantom	NA	SD, NPS, MTF	DLR images had lower noise, and high-contrast spatial resolution and task-based detectability were better than those of FBP, HIR, and MBIR
Jensen et al (96)	2022	TrueFidelity	Liver	Patient	51	SD, CNR, SNR	Compared with FBP, DLR improved image quality at 65% radiation dose reduction while preserving detection of liver lesions larger than 0.5 cm
Parakh et al (41)	2021	TrueFidelity	Liver	Patient	50	SD, CNR	Compared with HIR, DLR had a higher CNR, even in large patients
Nakamura et al (80)	2021	AiCE	Liver	Patient	72	SD, CNR	Lower dose DLR images were superior to standard-dose HIR images quantitatively and qualitatively at abdominal ultrahigh-resolution CT
Park et al (97)	2022	ClariCT.AI	Liver	Patient	80	SD, CNR, SNR, NPS	Lower-dose CT using DLD, at 67% dose reduction, provided noninferior overall image quality compared with standard-dose CT using MBIR

Table 2 (*continues*)

Table 2 *(continued)*: Noteworthy Studies on Deep Learning Reconstruction for CT Imaging

Author	Year	DLR Name	Application	Study Type	No. of Patients	Objective Metrics	Main Finding
Tamura et al (9)	2021	AiCE	Liver	Patient	90	SD, CNR	Objective and subjective image quality of DLR was found to be superior to that of MBIR and FBP at lower-dose abdominal CT
Nam et al (48)	2021	TrueFidelity	Liver	Patient	100	SD, CNR, SNR, ERD	With <50% radiation dose, DLR applied to contrast-enhanced chest CT exhibited better image noise and SNR than standard abdominal CT with HIR
Singh et al (42)	2020	AiCE	Liver	Patient	59	SD, SNR	Compared with FBP, HIR, and MBIR, DLR had higher image quality and lesion detection at chest and abdominopelvic CT at doses below 1 mSv
Nakamura et al (33)	2019	AiCE	Liver	Patient	58	SD, CNR	DLR improved image quality of abdominal CT for the evaluation of hypovascular hepatic metastases
Akagi et al (32)	2019	AiCE	Liver, aorta, portal vein	Patient	20	SD, CNR	Image noise and overall image quality for hepatic ultrahigh-resolution CT images improved with DLR as compared with HIR and MBIR
Greffier et al (98)	2022	AiCE, TrueFidelity	Lung	Phantom	NA	SD, NPS	Compared with FBP, both DLR algorithms reduced the image noise and improved lesion detectability
Nam et al (35)	2021	TrueFidelity, ClariCT.AI	Lung	Patient	100	SD, SNR, ERD	A vendor-agnostic DLD applied to lower-dose chest CT exhibited the best image quality compared with vendor-specific DLR and HIR
Mikayama et al (71)	2022	AiCE	Lung	Phantom	NA	SD	DLR showed higher accuracy compared with MBIR and HIR for the volumetric measurement of ground-glass nodules at lower-dose CT
Brady et al (49)	2021	AiCE	Pediatric	Patient, phantom	19	NPS	DLR improved image quality and dose reduction compared with FBP and HIR without sacrificing noise texture and spatial resolution
Sun et al (43)	2021	TrueFidelity	Pediatric	Patient	33	SD, CNR, SNR	Image quality of low-dose and contrast volume chest CT angiography was improved with high-setting DLR
Szczykutowicz et al (30)	2021	TrueFidelity	Protocol optimization	Phantom	NA	Noise, CNR, MTF, NPS	DLR maintained an FBP-like noise texture, whereas HIR shifted the NPS to lower frequencies
Cheng et al (47)	2021	TrueFidelity	Urography	Patient	52	SD, CNR, SNR	Compared with HIR, DLR used in CT urography reduced the radiation dose by 71% while maintaining image quality

Note.—From 70 studies, a selection of 26 noteworthy studies was made based on study design (prospective over retrospective), application (the number of studies per application in this table represents the available studies on this application), and number of patients in the study (a study with more patients was preferred if equivalent studies were found). AI = artifact index, AiCE = Advanced Intelligent Clear-IQ Engine, CNR = contrast-to-noise ratio, DLD = deep learning–based denoiser, DLR = deep learning reconstruction, ERD = edge-rise distance, FBP = filtered back projection, HIR = hybrid iterative reconstruction, MTF = modulation transfer function, MBIR = model-based iterative reconstruction, NA = not applicable, NPS = noise power spectrum, SD = standard deviation of the CT numbers in a region of interest, SNR = signal-to-noise ratio, SP = system performance, VMS = virtual monochromatic spectral.

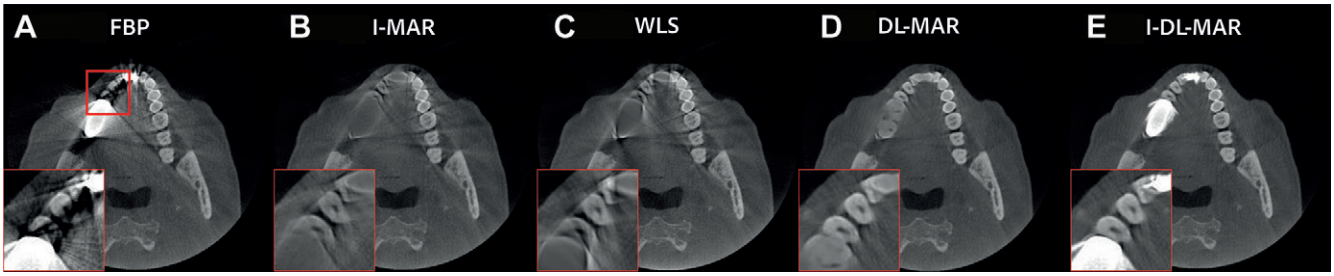

Figure 7: Images in a patient with a metal dental implant. Images were reconstructed with **(A)** filtered back projection (FBP), **(B)** interpolation metal artifact reduction (I-MAR), **(C)** weighted least square (WLS) iterative reconstruction, **(D)** deep learning metal artifact reduction (DL-MAR), and **(E)** sequential combination of I-MAR and DL-MAR (I-DL-MAR). The zoomed-in inset from the upper red box in image **A** shows shading and streak artifacts. The red boxes in images **B**, **C**, **D**, and **E** show the restoration of metal artifacts. Note the clear restoration quality of I-DL-MAR in image **E**. Reprinted, with permission, from reference 56.

images than in HIR and MBIR images. Correspondingly, DLR images were scored better by the readers.

Image Noise in Lower-Dose Protocols

In lower-dose CT studies, DLR algorithms showed excellent performance in image noise reduction. The image quality of DLR images was comparable with that of routine-dose scans reconstructed with either FBP or IR. Radiation dose reductions ranged from 30% to 71% (HIR vs DLR) and more than 50% (FBP vs DLR) (37,46–49).

Image Noise in Thin-Section Protocols

Image noise is influenced by section thickness (50). Thick sections reduce image noise but result in blurred tissue interfaces, which can affect image interpretation. In applications with small structures, such as coronary CT angiography and temporal bone CT imaging, thin sections can reveal more image features compared with thick sections. Some studies compared the image quality of thin-section DLR images with thick-section FBP or IR images. DLR algorithms maintained diagnostic image quality even in thin sections (30,31,49,50). For instance, Njølstad and colleagues (50) reported similar noise magnitude and contrast-to-noise ratio, as well as superior subjective image quality of 0.625-mm DLR images compared with 2.5-mm HIR images. Image quality assessed by three readers was perceived to be better due to improved noise texture, reduced artifacts, and sharper images.

Additionally, and equally important, the noise texture of DLR images was similar to that of ground truth images used in the training data set. For instance, when DLR algorithms were trained with FBP as the ground truth, DLR images had a similar noise texture to FBP. This resemblance positively affected the diagnostic confidence of readers, who were more confident in detecting liver lesions with DLR than MBIR, especially in low-contrast examinations (37).

Artifacts

Artifacts, such as beam-hardening and scatter artifacts, are commonly encountered in CT imaging and are difficult to correct for because they are often caused by the intrinsic physical or statistical behavior of photons (51). Several studies compared the presence of artifacts between images reconstructed with DLR and IR. Whereas some investigators did not find differences (34,41,44,47,52), others found artifacts slightly reduced with DLR (45,48,53,54).

Artifacts caused by metallic implants, such as dental fillings and orthopedic hardware, appear as bright and dark streaks across the reconstructed image. These artifacts obscure metallic implants and adjacent tissue, potentially leading to image misinterpretation or missed findings (55). Metal artifacts are caused by a combination of mechanisms, including photon starvation and beam hardening (51). Current metal artifact reduction (MAR) algorithms include normalized MAR and linear interpolation (55).

Metal Artifacts

In the past 5 years, deep learning–based MAR has been investigated. These algorithms are constructed similarly to image-based and hybrid DLR algorithms (ie, indirect). Image-based algorithms remove either primary metal artifacts or secondary artifacts introduced when MAR uses linear interpolation. They do this by feeding the artifact-corrupted image into the deep learning network (56). Hybrid algorithms first use a deep learning network before image reconstruction to identify, remove, and replace sinogram data corrupted by metallic implants. This approach often introduces secondary artifacts in the image, which are different than linear interpolation and are removed by a second network (Fig 7). Because artifact-corrupted and artifact-free matched training data are difficult to obtain but necessary for supervised learning, simulated artifacts are added to artifact-free data (57–59). However, since simulated metal artifacts may not accurately model real clinical artifacts, some authors have proposed an unsupervised learning method (60–62). In unsupervised learning, the algorithm learns by grouping data based on image features; hence, the training does not require matched data (62). Most MAR methods are available as a standalone framework for CT scans depicting metallic objects. Therefore, hybrid MAR algorithms requiring sinograms as input are limited to CT scans where the sinograms are accessible.

Studies investigating deep learning MAR algorithms are listed in Table 3. The majority of these studies compared the performance of one deep learning MAR algorithm with a cluster of non–deep learning algorithms and other deep learning MAR algorithms (supervised and unsupervised learning) (56–66). In general, these studies showed that deep learning MAR

Table 3: Studies on Deep Learning–based Metal Artifact Reduction for CT Imaging

Author	Year	Algorithm Name	Algorithm Type	Learning Type	Application
Lee et al (62)	2021	cycleGAN	Image-based	Supervised	Not specified
Wang et al (57)	2022	DICDNet	Image-based	Supervised	Pelvic
Yu et al (61)	2021	NA	Hybrid	Unsupervised	Not specified
Wang et al (63)	2021	DAN-Net	Hybrid	Supervised	Not specified
Lyu et al (66)	2020	DuDoNet++	Hybrid	Supervised	Not specified
Peng et al (64)	2020	NA	Hybrid	Supervised	Dental, hip, spinal
Liao et al (60)	2020	ADN	Image-based	Unsupervised	Not specified
Liang et al (56)	2019	I-DL-MAR	Image-based	Unsupervised	Dental
Gjesteby et al (58)	2019	DestreakNet-MSE	Image-based	Supervised	Pelvic, spinal
Huang et al (65)	2018	RL-ARCNN	Image-based	Supervised	Cervical
Zhang and Yu (59)	2018	CNNMAR	Image-based	Supervised	Not specified

Note.—ADN = artifact disentanglement network, CNNMAR = convolutional neural network–based metal artifact reduction, cycleGAN = cycle generative adversarial network, DAN-Net = dual-domain adaptive-scaling nonlocal network, DICDNet = deep interpretable convolutional dictionary network, DuDoNet++ = dual-domain network, I-DL-MAR = sequential combination of interpolation metal artifact reduction and deep learning metal artifact reconstruction, MSE = mean square error, NA = not applicable, RL-ARCNN = residual learning artifact reduction based on convolutional neural network.

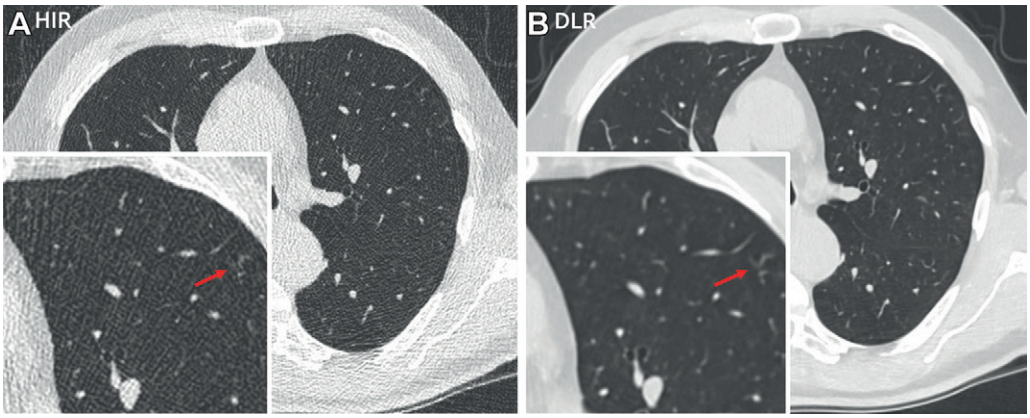

Figure 8: Axial contrast-enhanced CT scans of the chest. Lung screening was performed in an adult patient with a history of smoking. Images were acquired at 80 kVp and a volumetric CT dose index of 0.8 mGy and reconstructed with **(A)** 1-mm hybrid iterative reconstruction (HIR) and **(B)** 1-mm Precise Image (a direct deep learning reconstruction [DLR] algorithm). Streak artifacts from bone tissue are present in image **A** and reduce visualization of small vessels in the lungs (arrow). The artifact-reducing capabilities of DLR result in less pronounced streak artifacts than in HIR. Small vessels are more visible in image **B** than in **A** (arrow).

outperformed non–deep learning MAR algorithms (normalized MAR and linear interpolation) in peak signal-to-noise-ratio and structural similarity. Structural similarity is used to measure the similarity between two images, where one image is the reference image. Larger values of peak signal-to-noise ratio and structural similarity imply closer resemblance between the ground truth and optimized images, indicating more artifact-reducing capabilities (64). Peak signal-to-noise ratios and structural similarity values were larger with supervised learning than unsupervised learning (60,61).

Overall, DLR can be used to reduce artifacts. However, its performance in artifact reduction was similar to that of IR. Future studies should investigate whether FBP or MBIR images as ground truth and direct or indirect DLR algorithms result in fewer artifacts. For metal artifact removal, deep learning MAR removes metal artifacts more effectively than non–deep learning MAR, but larger clinical studies are necessary to evaluate the performance of individual deep learning MAR algorithms.

Clinical Applications of DLR

DLR has been tested in different imaging subdomains; a list of noteworthy DLR studies can be found in Table 2.

Brain

Image noise and beam-hardening and streak artifacts are common issues in brain imaging and can affect image interpretation, in particular for gray and white matter differentiation and hemorrhage detection (67). Two studies investigated the image quality of routine-dose noncontrast brain CT images reconstructed with indirect image-based DLR and direct DLR algorithms, respectively. Both studies reported improved image noise, artifact reduction, and gray and white matter differentiation with DLR compared with HIR. The indirect DLR algorithm was also compared with MBIR and had similar results (34,53).

Chest and Cardiac

In principle, lower-dose CT imaging is facilitated by the naturally high contrast of the chest tissues (Fig 8) (68). Recent studies reported improved image quality (signal-to-noise ratio, contrast-to-noise ratio, sharpness, and noise texture) with DLR compared with both HIR and MBIR in chest CT scans (35,45,69,70). Mikayama et al (71) used a phantom equipped with artificial nodules to compare the volumetric measurement error of HIR, MBIR, and DLR. In comparison with the true nodule volume, the volumetric measurement error of DLR was significantly lower than that of HIR and MBIR (1.4%, 8.0%, and 7.3%,

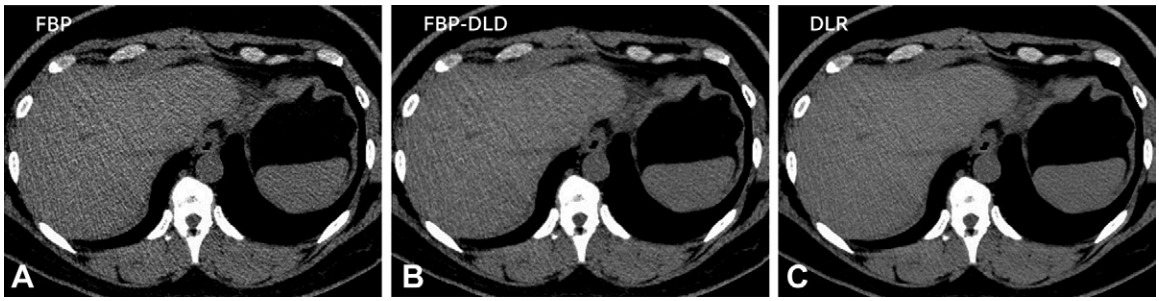

Figure 9: Unenhanced axial abdominal CT images in a 39-year-old woman admitted for nausea, vomiting, and abdominal pain show no abnormalities. Images were acquired at 120 kVp with a volumetric CT dose index of 33.6 mGy and reconstructed with **(A)** 1.25-mm filtered back projection (FBP) standard kernel, **(B)** 1.25-mm PixelShine deep learning–based denoising (DLD) applied to FBP standard kernel, and **(C)** 1.25-mm TrueFidelity deep learning reconstruction (DLR)–low weight standard kernel. Deep learning–based denoising and DLR reduced noise magnitude in reconstructions **B** and **C**, respectively, and improved heterogeneous liver parenchymal texture evaluation. Arm-down scanning resulted in streak artifacts in reconstructions **A** and **B**. These artifacts were reduced in the vendor-specific DLR in reconstruction **C**.

respectively) due to the superior noise texture and ability to maintain spatial resolution in lower-dose conditions (0.2 mSv). However, in a comparison between HIR, deep learning–based denoising, and DLR, Nam et al (35) found more distortion artifacts with DLR, manifesting as false miliary lung nodules and false granular mediastinal nodules.

In cardiac and vascular CT applications, contour delineation of small vessels has been reported as acceptable in routine-dose FBP, HIR, and MBIR but can be degraded at lower-dose scanning because of higher noise, lower spatial resolution, and blotchy noise texture (72,73). DLR has the potential to overcome this problem. Bernard et al (74) compared the radiation dose and image quality of HIR and DLR in 296 patients who underwent cardiac CT angiography to rule out a cardioembolic cause of stroke. Compared with HIR, DLR allowed for a dose reduction of 40% (volumetric CT dose index, 6.9 mGy for DLR vs 11.5 mGy for HIR) while improving the signal-to-noise ratio and contrast-to-noise ratio by 50%. In another study, Benz et al (75) compared image quality and diagnostic accuracy for stenosis assessment of HIR and DLR in 43 patients who underwent coronary CT angiography, using invasive coronary angiography as a reference. DLR resulted in improved image quality compared with HIR but did not improve diagnostic accuracy.

Abdominal

Abdominal CT imaging is characterized by low-contrast tissue interfaces (Figs 9, 10). The plastic or blotchy appearance of high-strength IR hampers the detection of hepatic lesions (76). Yang et al (77) studied 42 patients who underwent contrast-enhanced liver CT to assess image quality and lesion detection. They showed superior subjectively assessed image quality with DLR compared with HIR in routine-dose protocols; however, no differences in lesion detection rates were found. Other studies reported better objective and subjective image quality and lesion detectability of DLR in lower-dose conditions than both FBP and HIR (9,42,73,78,79). However, Jensen et al (54) have voiced concern over possible blurring of small lesions and vessels in medium- and high-strength DLR images. Further evaluation of DLR in prospective lesion detection and characterization studies is needed to determine if this blurring impacts diagnostic performance.

Overall, phantom and patient studies have suggested that DLR is favorable over other reconstruction techniques to achieve high-quality images in lower-dose abdominal CT due to substantially improved noise reduction, noise texture, and low-contrast spatial resolution.

Pediatric

In the pediatric population (Fig 11), low–radiation dose imaging is paramount. Sun and colleagues (43) compared the quality of images reconstructed with HIR and DLR in 33 children who underwent lower-dose chest cardiac CT angiography for pneumonia, neoplasm, lung malformation, or arteritis. DLR resulted in better subjective vascular delineation (3.7 of 5.0 vs 4.1 of 5.0), lower noise (29.5 HU vs 19.2 HU), and higher signal-to-noise ratio (14.6 vs 22.6) and contrast-to-noise ratio (13.7 vs 20.7). Brady et al (49) evaluated phantom-based scans and chest, abdominal, and pelvic CT examinations in children by comparing DLR with FBP, HIR, and MBIR. In the phantom analysis, object detectability and detection accuracy in DLR images were superior to those in other reconstruction techniques. In the image quality analysis of patient examinations, the DLR algorithm performed best for image noise, sharpness, object conspicuity, and radiologist confidence that the structure was correctly identified. Moreover, the potential dose reduction of DLR was estimated at 52% compared with HIR.

Challenges and Prospects of DLR

Challenges

A new image reconstruction technique like DLR needs a thorough assessment of image quality and diagnostic performance before replacing conventional techniques. Although comparisons of image quality parameters showing contrast-to-noise ratio and noise are important, new techniques should be driven by clinical superiority (eg, showing improved detection of specific lesions previously difficult to detect). This is especially relevant for DLR algorithms because deep learning networks are highly complex and use models that are not always fully interpretable.

Nonlinearities built into algorithms could introduce incorrect anatomic or pathologic features, particularly in low-dose settings. These artifacts may be introduced when a network incorrectly recognizes noise as a missing object in the image and replaces it with a nonexistent object (81). This phenomenon is known as hallucination (82). On the other hand, networks could also remove parts of the image incorrectly. We refer to this other phenomenon as inverse hallucination. For example, when small vessels or uncommon lesions are underrepresented in training data, these might be removed or blurred (32). Hallucinations and inverse hallucinations potentially result in false-positive and false-negative findings, respectively, in seemingly high-quality images (83).

One way to address this limitation is to focus on the quality of training data. Because artificial intelligence performance relies heavily on the training process, large training data sets with variability in patient demographics, clinical conditions, CT scanner models, and acquisition and reconstruction parameters may limit the problem (84). Large and heterogeneous training data sets are essential for the development of DLR algorithms but are notoriously hard to collect because of the associated costs and time requirements (14). Furthermore, robust testing of the networks with a variety of clinical inputs is also necessary (85).

The majority of currently available studies

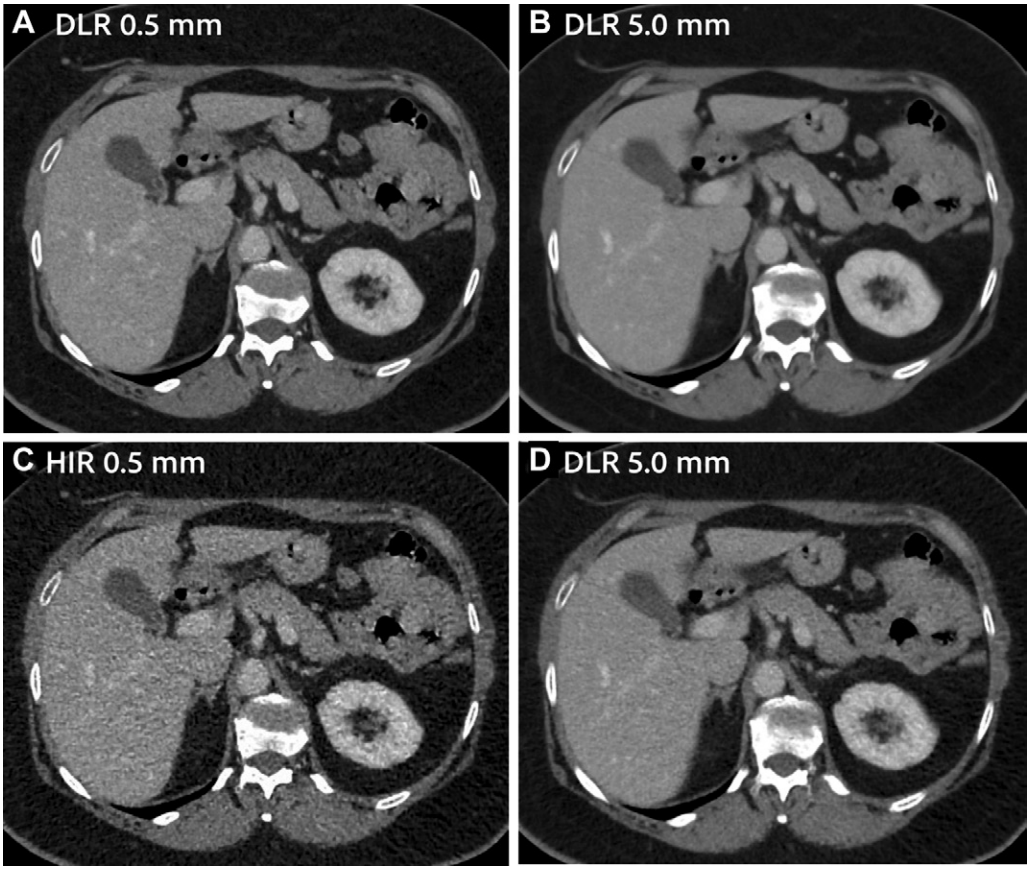

Figure 10: Contrast-enhanced axial abdominal CT images in a 63-year-old woman with recurrent endometrial carcinoma. Images were acquired at 120 kVp and 343 mA and reconstructed with **(A)** 0.5-mm Advanced Intelligent Clear-IQ Engine (AiCE), **(B)** 5.0-mm AiCE, **(C)** 0.5-mm hybrid iterative reconstruction (HIR), and **(D)** 5.0-mm HIR. AiCE is an indirect image-based deep learning reconstruction (DLR) algorithm. Thin sections in reconstructions **A** and **C** preserved spatial resolution but had more image noise compared with thick sections in reconstructions **B** and **D**. AiCE keeps image noise low in thin sections, whereas HIR leads to unacceptable higher levels of noise in 0.5-mm images.

Figure 11: Contrast-enhanced axial abdominal CT images in a 2-year-old boy after chemotherapy for hepatoblastoma show multiple areas of necrosis within the hepatic tumor. Images were acquired at 80 kVp with a volumetric CT dose index of 1.79 mGy and reconstructed with **(A)** 3.75-mm hybrid iterative reconstruction (HIR) standard kernel, **(B)** 1.25-mm HIR standard kernel, and **(C)** 1.25-mm TrueFidelity deep learning reconstruction (DLR)–high weight standard kernel. TrueFidelity is a direct DLR algorithm. Thin-section HIR in image **B** shows reduced low-contrast detectability and lesion delineation due to elevated image noise and deteriorated noise texture. Thin-section DLR in image **C** mimics the thicker-section HIR in image **A** in terms of image noise but shows improved spatial resolution.

using DLR focus on image quality and dose reduction. For a limited number of tasks (eg, lesion detection and lung nodule volumetry), the diagnostic performance of DLR has been compared with that of other reconstruction techniques. However, for many applications, the diagnostic performance of DLR is not known. More prospective studies focusing on the diagnostic performance of DLR are essential to evaluate its full potential. In particular, the diagnostic effect of possible blurring of small structures is an important unknown.

Artifact reduction is currently limited, but DLR has the potential to further reduce artifacts. It is yet not clear whether the use of FBP or MBIR images as ground truth and direct or indirect DLR algorithms result in fewer artifacts. More matched artifact-corrupted and artifact-free data included in the training phase can reduce artifacts even further.

Image characteristics, such as noise texture and artifact reduction, of different DLR algorithms can vary. These variations complicate the comparison of CT examinations acquired and reconstructed on scanners from different vendors, specifically in serial imaging. There is a need for enhanced vendor partnerships to reduce variations in image characteristics. However, because most algorithms are still proprietary, there is a need for standardization in the size of training sets, countries from which the data were obtained, and types of pathologic abnormalities.

Imaging in bariatric patients is challenging because a higher dose is required to produce diagnostically valuable images. DLR has the potential to keep noise and radiation doses low. To date, no bariatric studies with DLR have been conducted. Studies on large-patient scans reconstructed with DLR are needed.

Phantoms used for quality assurance of CT scanners might not be represented in the training data. Therefore, results from quality assurance tests may not be accurate. Manufacturers of CT phantoms need to make data of their phantom available to DLR algorithm developers. With these data, networks can be trained to accurately reconstruct the phantom.

With the introduction of techniques such as tube current modulation and MBIR, studies reported a potential dose reduction of about 50%–70%, similar to what has been presented for DLR (86,87). However, these reductions ended up being more moderate in the clinical setting. One needs to be aware that a reduction of 70% might only be possible in exceptional cases.

Future Prospects

Photon-counting CT is a highly promising technique that results in images with less noise, higher spatial resolution, and better spectral separation (88). By providing these high-quality images, photon-counting CT has the potential to further improve ground truth image quality and therefore improve the overall performance of DLR. Photon-counting CT may also benefit from DLR algorithms at various levels, from acquisition to image reconstruction and material decomposition. For example, networks applied to the raw data could extract low-level features and use this information for material decomposition even after image reconstruction. With more spectral information in the raw data, photon-counting CT reconstruction techniques await extremely complex tasks, and DLR has the potential to translate this into clinical practice.

CT imaging aims to provide as much diagnostic information as possible. Correctly acquired raw data contain all the information needed to formulate a diagnosis. However, raw data are not interpretable by humans, and image reconstruction is required for image interpretation. During the reconstruction process, some information might be lost due to suboptimal reconstruction methods (78). Deep learning algorithms can learn artificial decision-making from the raw data, as long as informative features needed for a decision are represented in the training data. Therefore, interpretation of the sinogram with use of deep learning is possible without image reconstruction. This can be used in an emergency setting, where the timely assessment of a CT scan is of the essence. Three studies showed the feasibility of analyzing CT sinograms with deep learning without image reconstruction for intracranial hemorrhage detection (89), cranial abnormalities (90), and blood vessel detection and characterization (91). To our knowledge, these are of yet the only studies on CT analysis without image reconstruction; further studies are needed.

Conclusion

Deep learning reconstruction (DLR) algorithms can be applied in the raw data domain, image domain, or a combination of both. The recent clinical introduction of DLR algorithms has demonstrated the potential of DLR to rapidly reconstruct images with low noise, desired noise texture, and preserved spatial resolution while providing the opportunity to reduce radiation dose up to 71%. Compared with filtered back projection and hybrid iterative reconstruction techniques, DLR allows for overall image quality improvement. Large heterogeneous training data sets and the use of photon-counting CT as ground truth have the potential to further improve DLR image quality, dose reduction, and artifact reduction. In the future, we anticipate deep learning to play a pivotal role in processing CT raw data containing spectral information.

Disclosures of conflicts of interest: L.R.K. No relevant relationships. **D.M.** Grant from the National Institute of Biomedical Imaging and Bioengineering (no. 5T32EB009035); consulting fees from Segmed; stock or stock options in Segmed; member of the trainee editorial board for *Radiology: Cardiothoracic Imaging*. **T.P.S.** Research support from Canon Medical Systems and GE Healthcare; consulting fees from Alara Imaging, Imalogix, Flowhow, Aidoc, and Asto CT/Leo Cancer Care; royalties from Medical Physics Publishing and royalties related to intellectual property from Flowhow and Qaelum. **N.R.v.d.W.** No relevant relationships. **A.S.W.** Research support from GE Healthcare, Siemens Healthineers, Varex Imaging, and the National Institutes of Health. **V.S.** No relevant relationships. **A.J.v.d.M.** Royalties from Thieme Verlag; payment for lectures from Guerbet; support for travel from Guerbet. **D.F.** Grant to institution from Siemens Healthineers; deputy editor for *Radiology: Cardiothoracic Imaging*. **M.J.W.** Research grant from the American Heart Association; consulting fees from Segmed; payment for expert testimony from Guidepoint; unpaid member of the Society of Cardiovascular Computed Tomography Corporate Relations Committee; stock or stock options in Segmed.

References

1. Kak AC, Slaney M. Principles of Computerized Tomographic Imaging. Society for Industrial and Applied Mathematics, 2001.
2. Gordon R, Bender R, Herman GT. Algebraic reconstruction techniques (ART) for three-dimensional electron microscopy and x-ray photography. J Theor Biol 1970;29(3):471–481.
3. Willemink MJ, Noël PB. The evolution of image reconstruction for CT – from filtered back projection to artificial intelligence. Eur Radiol 2019;29(5):2185–2195.
4. Uffmann M, Schaefer-Prokop C. Digital radiography: the balance between image quality and required radiation dose. Eur J Radiol 2009;72(2):202–208.

5. Willemink MJ, de Jong PA, Leiner T, et al. Iterative reconstruction techniques for computed tomography part 1: technical principles. Eur Radiol 2013;23(6):1623–1631.
6. Willemink MJ, Leiner T, de Jong PA, et al. Iterative reconstruction techniques for computed tomography part 2: initial results in dose reduction and image quality. Eur Radiol 2013;23(6):1632–1642.
7. Fleischmann D, Boas FE. Computed tomography—old ideas and new technology. Eur Radiol 2011;21(3):510–517.
8. Thibault JB, Sauer KD, Bouman CA, Hsieh J. A three-dimensional statistical approach to improved image quality for multislice helical CT. Med Phys 2007;34(11):4526–4544.
9. Tamura A, Mukaida E, Ota Y, Kamata M, Abe S, Yoshioka K. Superior objective and subjective image quality of deep learning reconstruction for low-dose abdominal CT imaging in comparison with model-based iterative reconstruction and filtered back projection. Br J Radiol 2021;94(1123):20201357.
10. Szczykutowicz TP. Optimizing Protocols for Today's Feature-Rich Scanners. Medical Physics Publishing, 2020.
11. LeCun Y, Bengio Y, Hinton G. Deep learning. Nature 2015;521 (7553):436–444.
12. Chartrand G, Cheng PM, Vorontsov E, et al. Deep learning: a primer for radiologists. RadioGraphics 2017;37(7):2113–2131.
13. Cheng PM, Montagnon E, Yamashita R, et al. Deep learning: an update for radiologists. RadioGraphics 2021;41(5):1427–1445.
14. Willemink MJ, Koszek WA, Hardell C, et al. Preparing medical imaging data for machine learning. Radiology 2020;295(1):4–15.
15. Bao P, Xia W, Yang K, et al. Convolutional sparse coding for compressed sensing CT reconstruction. IEEE Trans Med Imaging 2019;38(11):2607–2619.
16. Wu D, Kim K, El Fakhri G, Li Q. Iterative low-dose CT reconstruction with priors trained by artificial neural network. IEEE Trans Med Imaging 2017;36(12):2479–2486.
17. Yang Q, Yan P, Zhang Y, et al. Low-dose CT image denoising using a generative adversarial network with Wasserstein distance and perceptual loss. IEEE Trans Med Imaging 2018;37(6):1348–1357.
18. Kang E, Min J, Ye JC. A deep convolutional neural network using directional wavelets for low-dose x-ray CT reconstruction. Med Phys 2017;44(10):e360–e375.
19. Chen H, Zhang Y, Kalra MK, et al. Low-dose CT with a residual encoder-decoder convolutional neural network. IEEE Trans Med Imaging 2017;36(12):2524–2535.
20. Wolterink JM, Leiner T, Viergever MA, Isgum I. Generative adversarial networks for noise reduction in low-dose CT. IEEE Trans Med Imaging 2017;36(12):2536–2545.
21. Zhang Z, Yu L, Liang X, Zhao W, Xing L. TransCT: Dual-Path Transformer for Low Dose Computed Tomography. In: de Bruijne M, Cattin PC, Cotin S, et al, eds. Medical Image Computing and Computer Assisted Intervention – MICCAI 2021. MICCAI 2021. Lecture Notes in Computer Science, vol 12906. Springer, 2021; 55–64.
22. Zhu B, Liu JZ, Cauley SF, Rosen BR, Rosen MS. Image reconstruction by domain-transform manifold learning. Nature 2018;555(7697):487–492.
23. He J, Wang Y, Ma J. Radon inversion via deep learning. IEEE Trans Med Imaging 2020;39(6):2076–2087.
24. Ripley BD. Pattern Recognition and Neural Networks. Cambridge University Press, 2007.
25. Hsieh J, Liu E, Nett B, Tang J, Thibault JB, Sahney S. A new era of image reconstruction: TrueFidelity™ – Technical white paper on deep learning image reconstruction. 2019. https://www.gehealthcare.com/-/jssmedia/040dd213fa89463287155151fdb01922.pdf. Accessed December 10, 2021.
26. AI for significantly lower dose and improved image quality Precise Image: white paper. Philips. https://www.philips.com/c-dam/b2bhc/master/resource-catalog/landing/precise-suite/incisive_precise_image.pdf. Accessed December 15, 2021.
27. Boedeker K. AiCE Deep Learning Reconstruction: Bringing the power of Ultra-High Resolution CT to routine imaging. Canon Medical Systems. https://global.medical.canon/publication/ct/2019WP_AiCE_Deep_Learning. Accessed December 10, 2021.
28. Kim JH. Apparatus and method for denoising CT images. https://patents.google.com/patent/US9852527B2/en?assignee=claripi&oq=claripi. Published 2017. Accessed December 16, 2021.
29. PixelShine White Paper. WHAT'S THAT NOISE? AlgoMedica. https://www.algomedica.com/medical-imaging-resources#white-papers. Accessed February 24, 2022.
30. Szczykutowicz TP, Nett B, Cherkezyan L, et al. Protocol optimization considerations for implementing deep learning CT reconstruction. AJR Am J Roentgenol 2021;216(6):1668–1677.
31. Shirasaka T, Kojima T, Funama Y, et al. Image quality improvement with deep learning-based reconstruction on abdominal ultrahigh-resolution CT: a phantom study. J Appl Clin Med Phys 2021;22(7):286–296.
32. Akagi M, Nakamura Y, Higaki T, et al. Deep learning reconstruction improves image quality of abdominal ultra-high-resolution CT. Eur Radiol 2019;29(11):6163–6171. [Published correction appears in Eur Radiol 2019;29(8):4526–4527.]
33. Nakamura Y, Higaki T, Tatsugami F, et al. Deep learning-based CT image reconstruction: initial evaluation targeting hypovascular hepatic metastases. Radiol Artif Intell 2019;1(6):e180011.
34. Oostveen LJ, Meijer FJA, de Lange F, et al. Deep learning-based reconstruction may improve non-contrast cerebral CT imaging compared to other current reconstruction algorithms. Eur Radiol 2021;31(8):5498–5506.
35. Nam JG, Ahn C, Choi H, et al. Image quality of ultralow-dose chest CT using deep learning techniques: potential superiority of vendor-agnostic post-processing over vendor-specific techniques. Eur Radiol 2021;31(7):5139–5147. [Published correction appears in Eur Radiol 2021;31(8):6410.]
36. Hata A, Yanagawa M, Yoshida Y, et al. Combination of deep learning-based denoising and iterative reconstruction for ultra-low-dose CT of the chest: image quality and Lung-RADS evaluation. AJR Am J Roentgenol 2020;215(6):1321–1328.
37. Racine D, Brat HG, Dufour B, et al. Image texture, low contrast liver lesion detectability and impact on dose: deep learning algorithm compared to partial model-based iterative reconstruction. Eur J Radiol 2021;141:109808.
38. Kim Y, Oh DY, Chang W, et al. Deep learning-based denoising algorithm in comparison to iterative reconstruction and filtered back projection: a 12-reader phantom study. Eur Radiol 2021;31(11):8755–8764.
39. van Stiphout JA, Driessen J, Koetzier LR, et al. The effect of deep learning reconstruction on abdominal CT densitometry and image quality: a systematic review and meta-analysis. Eur Radiol 2022;32(5):2921–2929.
40. Solomon J, Lyu P, Marin D, Samei E. Noise and spatial resolution properties of a commercially available deep learning-based CT reconstruction algorithm. Med Phys 2020;47(9):3961–3971.
41. Parakh A, Cao J, Pierce TT, Blake MA, Savage CA, Kambadakone AR. Sinogram-based deep learning image reconstruction technique in abdominal CT: image quality considerations. Eur Radiol 2021;31(11):8342–8353.
42. Singh R, Digumarthy SR, Muse VV, et al. Image quality and lesion detection on deep learning reconstruction and iterative reconstruction of submillisievert chest and abdominal CT. AJR Am J Roentgenol 2020;214(3):566–573.
43. Sun J, Li H, Li J, et al. Improving the image quality of pediatric chest CT angiography with low radiation dose and contrast volume using deep learning image reconstruction. Quant Imaging Med Surg 2021;11(7):3051–3058.
44. Yoon H, Kim J, Lim HJ, Lee MJ. Image quality assessment of pediatric chest and abdomen CT by deep learning reconstruction. BMC Med Imaging 2021;21(1):146.
45. Hata A, Yanagawa M, Yoshida Y, et al. The image quality of deep-learning image reconstruction of chest CT images on a mediastinal window setting. Clin Radiol 2021;76(2):155.e15–155.e23.
46. Benz DC, Ersözlü S, Mojon FLA, et al. Radiation dose reduction with deep-learning image reconstruction for coronary computed tomography angiography. Eur Radiol 2022;32(4):2620–2628.
47. Cheng Y, Han Y, Li J, et al. Low-dose CT urography using deep learning image reconstruction: a prospective study for comparison with conventional CT urography. Br J Radiol 2021;94(1120):20201291.
48. Nam JG, Hong JH, Kim DS, Oh J, Goo JM. Deep learning reconstruction for contrast-enhanced CT of the upper abdomen: similar image quality with lower radiation dose in direct comparison with iterative reconstruction. Eur Radiol 2021;31(8):5533–5543.
49. Brady SL, Trout AT, Somasundaram E, Anton CG, Li Y, Dillman JR. Improving image quality and reducing radiation dose for pediatric CT by using deep learning reconstruction. Radiology 2021;298(1):180–188.
50. Njølstad T, Schulz A, Godt JC, et al. Improved image quality in abdominal computed tomography reconstructed with a novel deep learning image reconstruction technique – initial clinical experience. Acta Radiol Open 2021;10(4):20584601211008391.
51. Boas FE, Fleischmann D. CT artifacts: causes and reduction techniques. Imaging Med 2012;4(2):229–240.
52. Zeng L, Xu X, Zeng W, et al. Deep learning trained algorithm maintains the quality of half-dose contrast-enhanced liver computed tomography images: comparison with hybrid iterative reconstruction: study for the application of deep learning noise reduction technology in low dose. Eur J Radiol 2021;135:109487.
53. Kim I, Kang H, Yoon HJ, Chung BM, Shin NY. Deep learning-based image reconstruction for brain CT: improved image quality compared with adaptive statistical iterative reconstruction-Veo (ASIR-V). Neuroradiology 2021;63(6):905–912.

54. Jensen CT, Liu X, Tamm EP, et al. Image quality assessment of abdominal CT by use of new deep learning image reconstruction: initial experience. AJR Am J Roentgenol 2020;215(1):50–57.
55. Katsura M, Sato J, Akahane M, Kunimatsu A, Abe O. Current and novel techniques for metal artifact reduction at CT: practical guide for radiologists. RadioGraphics 2018;38(2):450–461.
56. Liang K, Zhang L, Yang H, Yang Y, Chen Z, Xing Y. Metal artifact reduction for practical dental computed tomography by improving interpolation-based reconstruction with deep learning. Med Phys 2019;46(12):e823–e834.
57. Wang H, Li Y, He N, Ma K, Meng D, Zheng Y. DICDNet: deep interpretable convolutional dictionary network for metal artifact reduction in CT images. IEEE Trans Med Imaging 2022;41(4):869–880.
58. Gjesteby L, Shan H, Yang Q, et al. A dual-stream deep convolutional network for reducing metal streak artifacts in CT images. Phys Med Biol 2019;64(23):235003.
59. Zhang Y, Yu H. Convolutional neural network based metal artifact reduction in x-ray computed tomography. IEEE Trans Med Imaging 2018;37(6):1370–1381.
60. Liao H, Lin WA, Zhou SK, Luo J. ADN: artifact disentanglement network for unsupervised metal artifact reduction. IEEE Trans Med Imaging 2020;39(3):634–643.
61. Yu L, Zhang Z, Li X, Ren H, Zhao W, Xing L. Metal artifact reduction in 2D CT images with self-supervised cross-domain learning. Phys Med Biol 2021;66(17):175003.
62. Lee J, Gu J, Ye JC. Unsupervised CT metal artifact learning using attention-guided β-CycleGAN. IEEE Trans Med Imaging 2021;40(12):3932–3944.
63. Wang T, Xia W, Huang Y, et al. DAN-Net: dual-domain adaptive-scaling non-local network for CT metal artifact reduction. Phys Med Biol 2021;66(15):155009.
64. Peng C, Li B, Liang P, et al. A cross-domain metal trace restoring network for reducing x-ray CT metal artifacts. IEEE Trans Med Imaging 2020;39(12):3831–3842.
65. Huang X, Wang J, Tang F, Zhong T, Zhang Y. Metal artifact reduction on cervical CT images by deep residual learning. Biomed Eng Online 2018;17(1):175.
66. Lyu Y, Lin WA, Lu J, Zhou SK. DuDoNet++: encoding mask projection to reduce CT metal artifacts. https://deepai.org/publication/dudonet-encoding-mask-projection-to-reduce-ct-metal-artifacts. Published January 1, 2020. Accessed September 2022.
67. Jones TR, Kaplan RT, Lane B, Atlas SW, Rubin GD. Single- versus multi-detector row CT of the brain: quality assessment. Radiology 2001;219(3):750–755.
68. Kubo T, Ohno Y, Takenaka D, et al; iLEAD study group. Standard-dose vs. low-dose CT protocols in the evaluation of localized lung lesions: capability for lesion characterization—iLEAD study. Eur J Radiol Open 2016;3:67–73.
69. Franck C, Zhang G, Deak P, Zanca F. Preserving image texture while reducing radiation dose with a deep learning image reconstruction algorithm in chest CT: a phantom study. Phys Med 2021;81:86–93.
70. Kim JH, Yoon HJ, Lee E, Kim I, Cha YK, Bak SH. Validation of deep-learning image reconstruction for low-dose chest computed tomography scan: emphasis on image quality and noise. Korean J Radiol 2021;22(1):131–138.
71. Mikayama R, Shirasaka T, Kojima T, et al. Deep-learning reconstruction for ultra-low-dose lung CT: volumetric measurement accuracy and reproducibility of artificial ground-glass nodules in a phantom study. Br J Radiol 2022;95(1130):20210915.
72. Higaki T, Nakamura Y, Zhou J, et al. Deep learning reconstruction at CT: phantom study of the image characteristics. Acad Radiol 2020;27(1):82–87.
73. Lee JE, Choi SY, Hwang JA, et al. The potential for reduced radiation dose from deep learning-based CT image reconstruction: a comparison with filtered back projection and hybrid iterative reconstruction using a phantom. Medicine (Baltimore) 2021;100(19):e25814.
74. Bernard A, Comby PO, Lemogne B, et al. Deep learning reconstruction versus iterative reconstruction for cardiac CT angiography in a stroke imaging protocol: reduced radiation dose and improved image quality. Quant Imaging Med Surg 2021;11(1):392–401.
75. Benz DC, Benetos G, Rampidis G, et al. Validation of deep-learning image reconstruction for coronary computed tomography angiography: impact on noise, image quality and diagnostic accuracy. J Cardiovasc Comput Tomogr 2020;14(5):444–451.
76. Singh S, Kalra MK, Hsieh J, et al. Abdominal CT: comparison of adaptive statistical iterative and filtered back projection reconstruction techniques. Radiology 2010;257(2):373–383.
77. Yang S, Bie Y, Pang G, et al. Impact of novel deep learning image reconstruction algorithm on diagnosis of contrast-enhanced liver computed tomography imaging: comparing to adaptive statistical iterative reconstruction algorithm. J XRay Sci Technol 2021;29(6):1009–1018.
78. Racine D, Becce F, Viry A, et al. Task-based characterization of a deep learning image reconstruction and comparison with filtered back-projection and a partial model-based iterative reconstruction in abdominal CT: a phantom study. Phys Med 2020;76:28–37.
79. Li LL, Wang H, Song J, Shang J, Zhao XY, Liu B. A feasibility study of realizing low-dose abdominal CT using deep learning image reconstruction algorithm. J XRay Sci Technol 2021;29(2):361–372.
80. Nakamura Y, Narita K, Higaki T, Akagi M, Honda Y, Awai K. Diagnostic value of deep learning reconstruction for radiation dose reduction at abdominal ultra-high-resolution CT. Eur Radiol 2021;31(7):4700–4709.
81. Cruz C, Foi A, Katkovnik V, Egiazarian K. Nonlocality-reinforced convolutional neural networks for image denoising. IEEE Signal Process Lett 2018;25(8):1216–1220.
82. Belthangady C, Royer LA. Applications, promises, and pitfalls of deep learning for fluorescence image reconstruction. Nat Methods 2019;16(12):1215–1225.
83. Zhao R, Zhang Y, Yaman B, Lungren MP, Hansen MS. End-to-End AI-based MRI Reconstruction and Lesion Detection Pipeline for Evaluation of Deep Learning Image Reconstruction. arXiv 2109.11524 [preprint] https://arxiv.org/abs/2109.11524. Posted September 23, 2021. Accessed September 2022.
84. Currie G, Rohren E. Social asymmetry, artificial intelligence and the medical imaging landscape. Semin Nucl Med 2022;52(4):498–503.
85. Qayyum A, Qadir J, Bilal M, Al-Fuqaha A. Secure and robust machine learning for healthcare: a survey. IEEE Rev Biomed Eng 2021;14:156–180.
86. Katsura M, Matsuda I, Akahane M, et al. Model-based iterative reconstruction technique for radiation dose reduction in chest CT: comparison with the adaptive statistical iterative reconstruction technique. Eur Radiol 2012;22(8):1613–1623.
87. Jakobs TF, Becker CR, Ohnesorge B, et al. Multislice helical CT of the heart with retrospective ECG gating: reduction of radiation exposure by ECG-controlled tube current modulation. Eur Radiol 2002;12(5):1081–1086.
88. Willemink MJ, Persson M, Pourmorteza A, Pelc NJ, Fleischmann D. Photon-counting CT: technical principles and clinical prospects. Radiology 2018;289(2):293–312.
89. Lee H, Huang C, Yune S, Tajmir SH, Kim M, Do S. Machine friendly machine learning: interpretation of computed tomography without image reconstruction. Sci Rep 2019;9(1):15540.
90. Hooper SM, Dunnmon JA, Lungren MP, et al. Impact of upstream medical image processing on downstream performance of a head CT triage neural network. Radiol Artif Intell 2021;3(4):e200229.
91. De Man Q, Haneda E, Claus B, et al. A two-dimensional feasibility study of deep learning-based feature detection and characterization directly from CT sinograms. Med Phys 2019;46(12):e790–e800.
92. Masuda S, Yamada Y, Minamishima K, Owaki Y, Yamazaki A, Jinzaki M. Impact of noise reduction on radiation dose reduction potential of virtual monochromatic spectral images: comparison of phantom images with conventional 120 kVp images using deep learning image reconstruction and hybrid iterative reconstruction. Eur J Radiol 2022;149:110198.
93. Sato M, Ichikawa Y, Domae K, et al. Deep learning image reconstruction for improving image quality of contrast-enhanced dual-energy CT in abdomen. Eur Radiol 2022;32(8):5499–5507.
94. Li W, Diao K, Wen Y, et al. High-strength deep learning image reconstruction in coronary CT angiography at 70-kVp tube voltage significantly improves image quality and reduces both radiation and contrast doses. Eur Radiol 2022;32(5):2912–2920.
95. Yi Y, Xu C, Xu M, et al. Diagnostic improvements of deep learning-based image reconstruction for assessing calcification-related obstructive coronary artery disease. Front Cardiovasc Med 2021;8:758793.
96. Jensen CT, Gupta S, Saleh MM, et al. Reduced-dose deep learning reconstruction for abdominal CT of liver metastases. Radiology 2022;303(1):90–98.
97. Park S, Yoon JH, Joo I, et al. Image quality in liver CT: low-dose deep learning vs standard-dose model-based iterative reconstructions. Eur Radiol 2022;32(5):2865–2874.
98. Greffier J, Frandon J, Si-Mohamed S, et al. Comparison of two deep learning image reconstruction algorithms in chest CT images: a task-based image quality assessment on phantom data. Diagn Interv Imaging 2022;103(1):21–30.